Operational Characteristics and Performance of the Disk-RDRE

Keon-Hyeong Lee, Min-Seon Jo, Gyeong-Ui Mo, Su-Wan Choi, Bu-Kyeng Sung, Jeong-Yeol Choi*
Department of Aerospace Engineering, Pusan National University
Busan, 46241, Republic of Korea

1 Introduction

Detonation-based propulsion systems employing the concept of Pressure Gain Combustion (PGC) have been actively studied worldwide during last decades to enhance the performance of power systems [1, 2]. Among these, Rotating Detonation Engines (RDE) have attracted significant attention due to their structural simplicity [3]. RDEs are being explored in various configurations, including annular, hollow, disk, and cone shapes [4-9]. In particular, disk or radial-shaped RDE offers the advantage of reducing length and mass of the rocket engine. As a result, recent experimental studies have focused on these disk- or radial-shaped RDE configurations [10, 11]. However, to use RDEs as rocket engines, it is necessary to reduce weight by omitting the central body and to develop an appropriate configuration that allows integration within the launch vehicle.

In this study, a disk-type Rotating Detonation Rocket Engine (disk-RDRE) without a central body was designed with an emphasis on minimizing its length and weight, and experimentally investigated its operational characteristics and propulsion performance. The operational characteristics of the disk-RDRE were investigated using high-speed camera and ICP-type dynamic pressure sensors, and its performance was evaluated through experiments with an average thrust of approximately 350 N.

2 Experimental Apparatus

The disk-RDRE configuration is shown in Fig. 1. The propellants used were gaseous ethylene (GC_2H_4) and oxygen (GO_2), which were supplied into the combustor through 90 hole-type impinging injectors. The injection angle of the propellant is 45 degrees for both the fuel and the oxidizer. The detonation channel height is 5.5 mm, and the combustor diameter is 100 mm. The nozzle throat area is 474.8 mm^2, and the nozzle expansion ratio is 2.726. The disk-RDRE was ignited using a pre-detonator (PD), which has a length of 270 mm and features an internal diameter tapering from 4.22 mm to 2 mm. The fuel and oxidizer used in the PD were also gaseous ethylene and oxygen. This PD has been validated through various previous research [12, 13]. The combustion duration was limited to 0.1–0.4 sec to protect the equipment.

Correspondence to: aerochoi@pusan.ac.kr

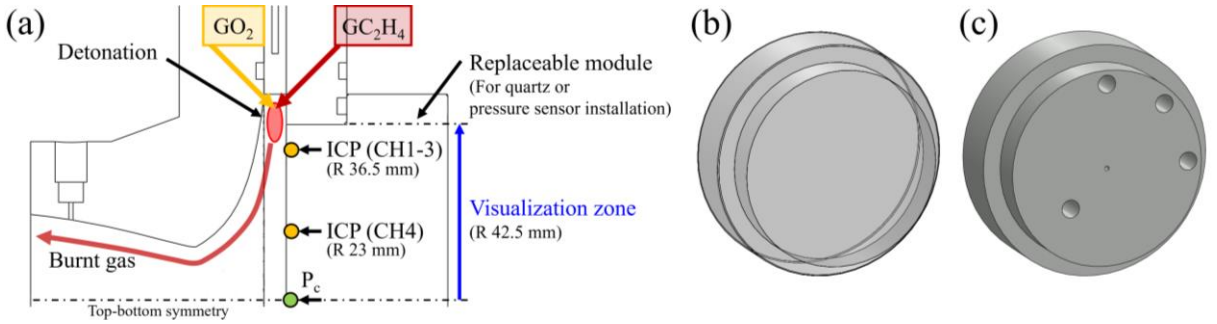

Figure 1: (a) Schematic of the disk-RDRE; (b) replaceable disk-shaped quartz window; (b) replaceable sensor module for installing dynamic and static pressure sensors.

To investigate the operational characteristics, a Phantom v2512 high-speed camera and PCB's 113B24 ICP-type dynamic pressure sensors were utilized. Disk-shaped quartz window was used to capture the flow features inside of the combustor, while the windows was replaced with sensor module with dynamic and static pressure sensors. Fig. 1 (b) and (c) shows the two replaceable modules. Under all conditions, the high-speed camera recorded at a resolution of 256 × 256 and a frame rate of 200,000 fps. High-speed camera images were post-processed to effectively illustrate the detonation propagation characteristics. Unwrapped images were generated using a post-processed method similar to that of Bennewitz et al [14, 15]., and luminosity data from a single pixel at 90% of the quartz window outer boundary were extracted for Fast Fourier Transform (FFT) and Short-Time Fourier Transform (STFT) analysis. Dynamic pressure sensor data were also analyzed using FFT and STFT to determine the operating frequency. The mass flow rate was measured using a FM153B series differential pressure mass flow meter from Enbac Company. Thrust was measured using a SBA-100 loadcell and a WTM-500 amplifier from CAS Corp.

3 Experimental Results

Table 1 presents the results of two representative experiments. Due to differences in analysis methods depending on the primary measurement device, the main measurement device was also documented.

Table 1: Summary of results for representative experimental conditions.

Case	$\dot{m}$ (g/s)*	Ø	$f_{operation}$ (kHz)	Mode	Max. thrust (N)	Main measurement
1	120.8	1.11	12.33	2-wave	287	High-speed camera
2	161.8	1.27	12.75	2-wave	373	ICP-type pressure sensor

*Differential-pressure mass flow meter measurement results

Fig. 2 and Fig. 3 presents the results for Case 1. Fig. 2 shows black-and-white inverted high-speed camera snapshots at each time point after the ignition of the disk-RDRE. Fig. 3 (a) shows an unwrapped image generated through post-processing from high-speed camera image, while Fig. 3 (b) is STFT and FFT results of extracted luminosity data. The unwrapped image allows for an easy observation of the operational characteristics after RDRE ignition. By drawing a vertical line (e.g. blue line) at a specific time point on the unwrapped image and counting the intersections, the number of propagating waves at that moment can be determined.

By comparing the unwrapped image with the black-and-white inverted snapshots, the disk-RDRE stabilization process can be observed as follows. Immediately after ignition, a strong transverse wave was generated by the PD. In annular-type RDREs, transverse waves do not appear during PD ignition

due to the presence of the center body. However, in coreless-RDRE, a strong transverse wave crossing the center of the combustor is generated by the PD. Subsequently, the detonation wave mode developed into a 3-wave mode maintained temporarily, and transitioned to 2-wave mode. When the transition process involving a decrease in wave number starts, the previously uniform distance between waves gradually becomes irregular. The transition becomes complete as a specific wave merged with an adjacent wave. The stable 2-wave mode appears after approximately 5 ms following ignition.

Performing STFT on the luminosity data allows for the identification of time-varying frequencies. As shown in Fig. 3 (b), a frequency of 16.53 kHz appears at 3-4 ms after ignition, and a consistent frequency of 12.33 kHz is observed from 6 ms onward. By comparing the snapshots with the STFT frequencies, it can be determined that the 16 kHz range frequency corresponds to the 3-wave mode, while the 12 kHz range frequency corresponds to the 2-wave mode. Therefore, observing frequency changes provides insight into whether a mode transition has occurred. In addition to the presented representative cases, a frequency of 12 kHz band was observed in all experiments when the disk-RDRE operated stably.

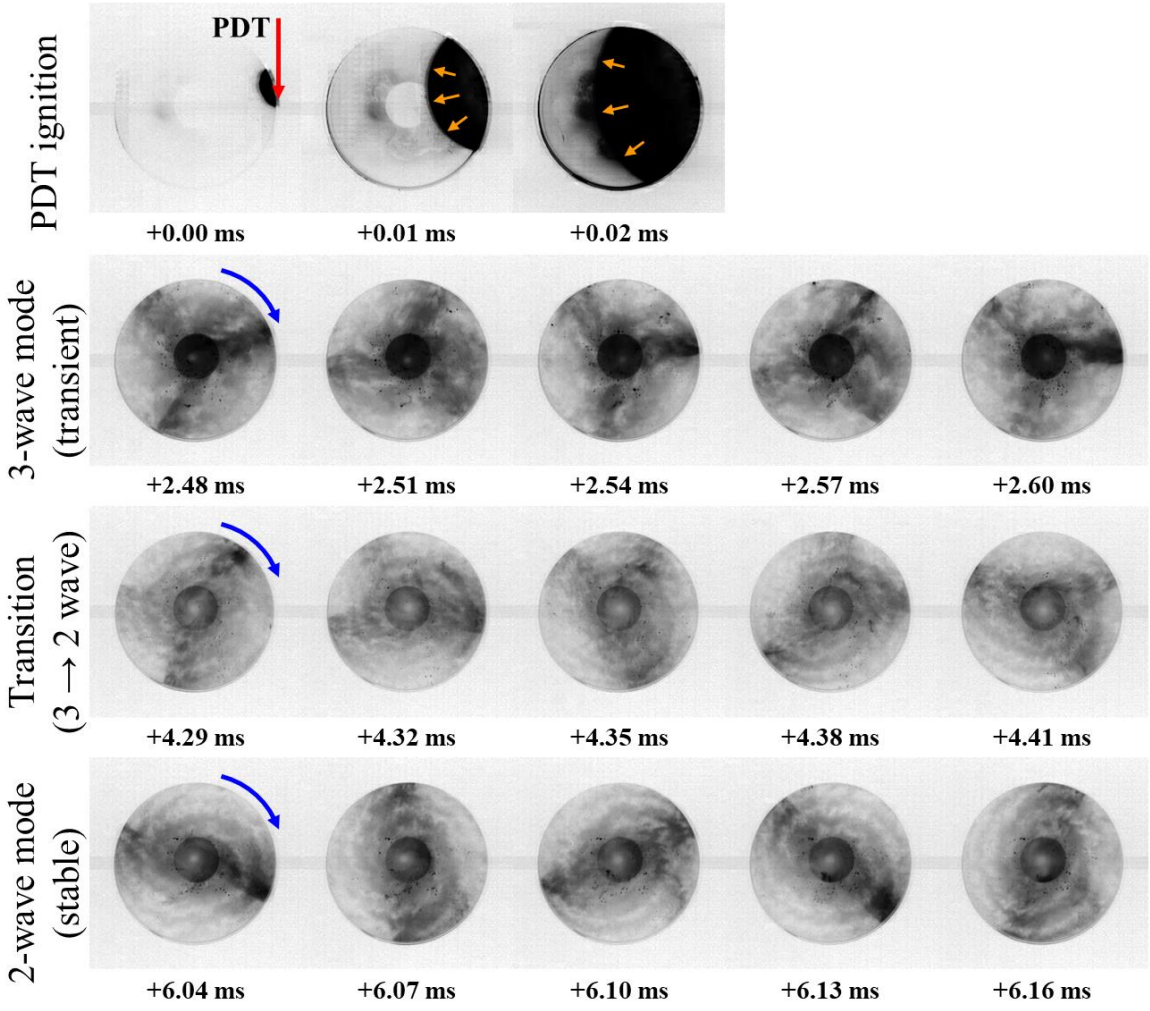

Figure 2: High-speed camera snapshots of Case 1 (black-and-white inverted).

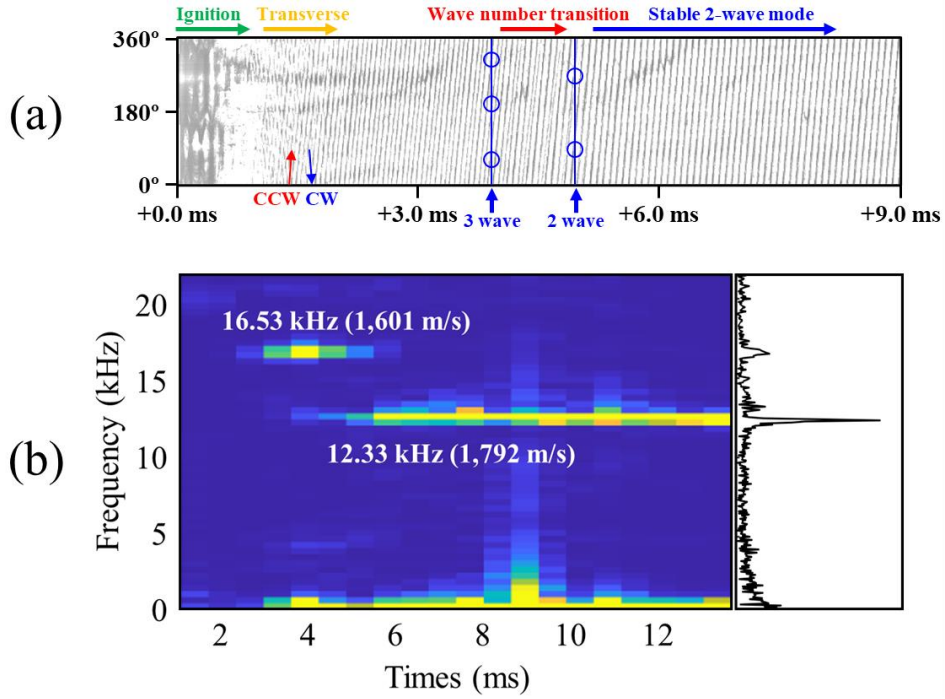

Figure 3: (a) Detonation propagation tracing (unwrapped image); (b) STFT and FFT results of extracted luminosity data (Case 1).

By analyzing the dynamic pressure sensor data using STFT method, higher resolution STFT results can be obtained compared to those from high-speed camera STFT results. Therefore, the dynamic pressure sensor data measured during the Case 2 experiment was analyzed using STFT and FFT methods to identify the operating frequencies. The results are shown in Fig. 4 (a).

Previously, it was inferred from the high-speed camera luminosity STFT results that a frequency of approximately 16 kHz was derived for the 3-wave mode, and a frequency of approximately 12 kHz was derived for the 2-wave mode. From Fig. 4 (a), a frequency of 12.75 kHz was measured in Case 2. This indicates that the 3-wave mode did not appear during the Case 2 combustion experiment, and the disk-RDRE operated stably in the 2-wave mode. Based on the confirmed stable operation of Case 2, the performance of the combustor was calculated. In addition, the measured combustion pressure for Case 2 is shown in Fig. 4 (b), and the measured thrust is presented in Fig. 4 (c).

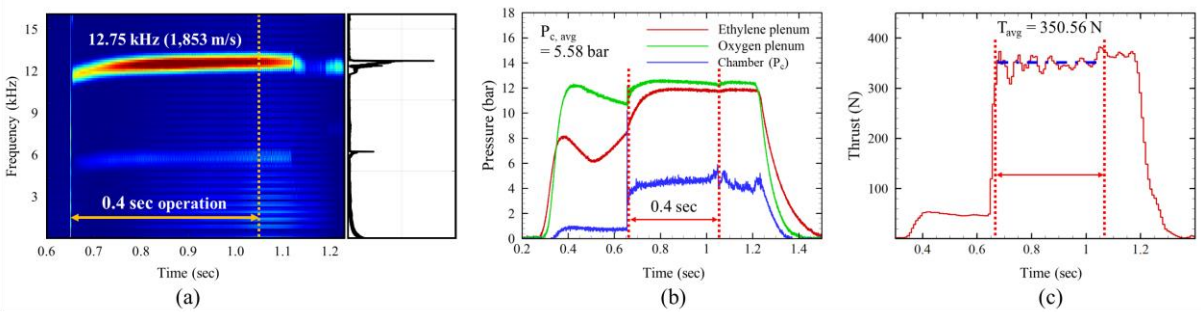

Figure 4: (a) STFT/FFT results of the dynamic pressure sensor data; (b) propellant plenum and combustion pressures; (c) measured thrust (Case 2).

Specific impulse (I_{sp}) was calculated based on the measured thrust and mass flow rate. There is a possibility that the differential pressure mass flow meter did not measure the mass flow rate accurately due to the short duration of the experiment. The I_{sp} was derived by comparing the mass flow rate measured during non-combustion and combustion experiments to address this issue. Due to the short combustion duration, there is a slight difference between the two methods of deriving the mass flow rate. The non-combustion experiment measured the mass flow rate by supplying propellant for 1 sec without combustion. Based on these results, an empirical correlation between the plenum pressure and mass flow rate was established. Using this correlation and the plenum pressure measured during combustion experiments, a non-combustion mass flow rate was estimated. This estimated value was then compared with the mass flow rate measured using a differential pressure flow meter during combustion. Fig. 5 (a) shows the estimated mass flow rate from the non-combustion experiment and the measured mass flow rate during the combustion experiment.

Fig. 5 (b) shows I_{sp} results for some experimental conditions. In Case 2 (relatively high $\dot{m}$), the average combustion pressure (P_c) was measured as 5.58 bar, and the average thrust was 350.56 N during the combustion duration of 0.4 sec. For this conditions, theoretical I_{sp} is 242.0 sec, while non-combustion I_{sp} is 203.3 sec and combustion I_{sp} is 231.5 sec. The theoretical I_{sp} was calculated using NASA CEA for a P_c of 5.6 bar. The combustion I_{sp} performance of 95.7% was achieved for this short time experiment. Although there is difference between the combustion and non-combustion results, it was understood that sufficient mass flow rate data could be obtained if the experiment is conducted for a duration long enough for the differential pressure flow meter to respond (approximately within 1 sec). It is also found that the method of analyzing performance by comparing non-combustion and combustion experiments was found to be reasonable.

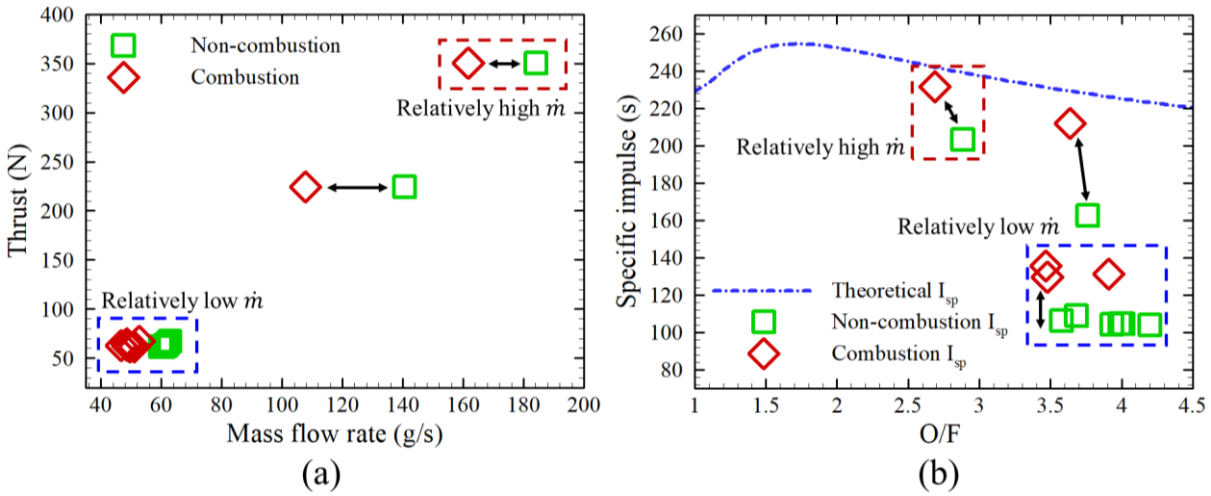

Figure 5: (a) Thrust according to mass flow rate; (b) specific impulse (I_{sp}) according to O/F ratio.

4 Conclusions

The operational characteristics of the disk-RDRE were investigated using high-speed camera and dynamic pressure sensors, and the combustor performance was calculated. The frequency analysis of high-speed camera images and dynamic pressure sensors confirmed that similar frequencies appeared depending on the wave mode. When operating in the 3-wave mode, a frequency of about 16 kHz was observed, while in the 2-wave mode, a frequency of about 12 kHz was observed. Additionally, when the operation of the disk-RDRE became stabilized, it converged to the 2-wave mode.

The disk-RDRE performance was calculated by measuring the combustion pressure, thrust, and mass flow rate. Although further research is needed to improve the method of calculating performance due to the error of the differential pressure mass flow meter and the short combustion duration, the performance was estimated by calculating the non-combustion I_{sp} and combustion I_{sp}. As a result, a combustion I_{sp} of about 95% relative to the theoretical I_{sp} was confirmed under relatively high mass flow conditions.

References

[1] Niyasdeen MN, Kim JM, Oh S, Choi JY. (2018). Review on the Research Progresses in Rotating Detonation Engine. Detonation Control for Propulsion, Shock Wave and High Pressure Phenomena, Springer 2018: 109-159.

[2] Yi TH, Lou J, Turangan C, Choi JY, Wolanski P. (2011). Propulsive Performance of a Continuously Rotating Detonation Engine. J. Prop. Pow. 27(1): 171-181.

[3] Kim JM, Niyasdeen MN, Han HS, Oh S, Choi JY. (2017). Research Activities on PGC Propulsion based on RDE, Part I: Basic Studies. J. Korean Soc. Prop. Eng. 21(5): 97-107.

[4] Han HS, Lee ES, Choi JY. (2021). Experimental Investigation of Detonation Propagation Modes and Thrust Performance in a Small Rotating Detonation Engine Using C_2H_4/O_2 Propellant. Energies 14(5): 1-20.

[5] Bykovskii FA, Zhdan SA, Vedernikov EF. (2006). Continuous Spin Detonations. J. Prop. and Pow. 22(6): 1204-1216.

[6] Kawalec M, Wolański P, Perkowski W, Bilar A. (2023). Development of a Liquid-Propellant Rocket Powered by a Rotating Detonation Engine. J. Prop. and Pow. 39(4): 554-561.

[7] Lee ES, Han HS, Choi JY. (2021). An Experimental Study of Tri-arc Rotating Detonation Engine Using Gaseous Ethylene/Oxygen. J. Korean Soc. Prop. Eng. 25(1): 19-28.

[8] Niyasdeen MN, Choi JY. (2025). Computational Study of Chemical Timescales in an Ethylene-Oxygen Non-Premixed RDE. AIAA SCITECH 2025 Forum, Orlando, FL, AIAA 2025-1182.

[9] Sung BK, Choi JY. (2025). Numerical Investigation on the Development of the Rotating Detonative Instability in a Rocket Combustor. AIAA SCITECH 2025 Forum, Orlando, FL, AIAA 2025-0403.

[10] Boller SA, Polanka MD, Huff R, Schauer F, Fotia M, Hoke J. (2019). Experimental Flow Visualization in a Radial Rotating Detonation Engine. AIAA Scitech 2019 Forum, San Diego, CA, AIAA 2019-1253.

[11] Ishii K, Ohno K, Kawana H, Kawasaki K, Hayashi AK, Tsuboi N. (2023). Operation characteristics of a disk-type rotating detonation engine. Shock waves 33: 267-274.

[12] Lee KH., Kim MS, Choi JY, Yu KH. (2024). An Experimental Investigation of Low-Frequency Active Excitation in Scramjet Combustor Using a Micro-Pulse Detonation Engine. Aerospace 11(7): 1-20.

[13] Mo GU, Koo IH, Lee KH, Choi SW, Choi JY. (2024). Effects of Fuel Penetration on the RDE Performance with JISC Injector Configuration. Aerospace 11(9): 1-17.

[14] Bennewitz JW, Bigler BR, Hargus WA, Danczyk SA, Smith RD. (2018). Characterization of Detonation Wave Propagation in a Rotating Detonation Rocket Engine using Direct High-Speed Imaging. 2018 Joint Propulsion Conference, Cincinnati, OH, AIAA 2018-4688.

[15] Koo IH, Lee KH, Kim MS, Han HS, Kim H, Choi JY. (2023). Effects of Injector Configuration on the Detonation Characteristics and Propulsion Performance of Rotating Detonation Engine (RDE). Aerospace 10(11): 1-15.